Research Square

Preprints are preliminary reports that have not undergone peer review.
They should not be considered conclusive, used to inform clinical practice,
or referenced by the media as validated information.

MODELING OF THE URBAN HEAT ISLAND IN AN AMAZONIAN CITY

Luciomar da Silva Almeida Filho

luciomar.almeida@unesp.br

Universidade Estadual Paulista (Unesp)

Luis Flávio de Araújo

Universidade Estadual Paulista (Unesp)

Margarete Cristiane de Costa Trindade Amorim

Universidade Estadual Paulista (Unesp)

João Cândido André da Silva Neto

Universidade Federal do Amazonas

Natacha Cintia Regina Aleixo

Universidade Federal do Amazonas

Research Article

Keywords: Urban climate, Multiple linear regression, Amazon rainforest, Local climate zones, Spatialization method, locally weighted mapping

Posted Date: November 11th, 2026

DOI: https://doi.org/10.21203/rs.3.rs-11146198/v1

License: This work is licensed under a Creative Commons Attribution 4.0 International License.
Read Full License

Additional Declarations: No competing interests reported.

MODELING OF THE URBAN HEAT ISLAND IN AN AMAZONIAN CITY

Luciomar da Silva Almeida Filho[1*], Luis Flávio de Araújo[1], Margarete Cristiane de Costa Trindade Amorim[1], João Cândido André da Silva Neto[2], Natacha Cintia Regina Aleixo[2]

*Correspondence
Luciomar da Silva Almeida Filho, luciomar.almeida@unesp.br

Abstract

The urban heat island (UHI) is a phenomenon specific to the urban climate, defined by the difference in air temperature recorded between a built-up/paved area and its natural/vegetated surroundings, and it has implications for the comfort and health of the urban population. The study's methodology involves collecting primary data using the moving transect technique during representative periods of the rainy and drier seasons in the city of Coari, with data collection taking place in September 2019 and 2023 and November 2024. Secondary data obtained through remote sensing and from institutional sources were used to create maps characterizing the urban area for application in statistical modeling to spatialize the UHI. The results demonstrate that in Coari, urban development has generated significant heat islands that vary depending on weather conditions and the local climate zones mapped in the city, with a modeled air temperature difference that can exceed 5 °C. The importance of this research lies in the fact that, in the Western Amazon, there is no observation network in urban environments, particularly in small cities such as Coari, that can support research on atmospheric changes at the local scale. The statistical modeling demonstrated the ability to represent the spatial variation observed in the analyzed transects, with performance that varied across the data collection dates in Coari, primarily because it allowed for a correlation between urban site characteristics and air temperature behavior; it also highlighted the need to consider other variables specific to the Amazonian context to obtain more meaningful results.

Keywords: Urban climate; Multiple linear regression; Amazon rainforest; Local climate zones; Spatialization method; locally weighted mapping.

Introduction

Environmental changes confronting humanity have become increasingly clear as the frequency of climate and weather extremes rises. Reports from the Intergovernmental Panel on Climate Change [1] show that human activities contribute to global warming through greenhouse gas emissions, which continue to increase in

[1] Department of Geography, School of Science and Technology, São Paulo State University Júlio de Mesquita Filho (UNESP), Educational Center, Presidente Prudente, São Paulo, Brazil.

[2] Department of Geography, Institute of Philosophy, Humanities, and Social Sciences, Federal University of Amazonas (UFAM), General Rodrigo Otávio Avenue, Coroado, Manaus, Amazonas, Brazil.

response to the unsustainable use of natural resources, consumption patterns, and production practices.

Globally, rising urban temperatures are linked to adverse impacts on human health, economic losses, service disruptions, and declines in social well-being. These effects disproportionately affect economically and socially marginalized populations [1].

At the local level, such changes are particularly significant because most of the world's population now lives in cities. The UN-Habitat World Cities Report [2] estimates that by 2050, 68 percent of the global population will live in urban areas. In Brazil, this proportion is even higher, reaching 84.36 percent of the total population [2]. These data reinforce the need to understand local and regional climates, which are altered by urbanization. Moreover, analyzing how energy exchanges occur within the urban climate system provides essential support for developing public policies that mitigate and address the effects of climate change in cities.

Urban climate can thus be understood as an open, unique, and complex system derived from the anthropogenic process of city building and the cumulative transformations of urban dynamics. It encompasses the climate of a given terrestrial area and its degree of urbanization. It consists of two sets of constituent elements – natural and social – and stands for a key component of environmental quality [3].

The urban heat island (UHI) is a phenomenon closely associated with urban climate formation. In warm regions, it exacerbates thermal discomfort, physiological stress, heat-related mortality, adaptation costs, and electricity consumption due to air-conditioning use [4,5,6].

The causes of UHIs are tied to the physical properties of construction materials, urban morphology, and human activities. Low proportions of permeable surfaces, limited vegetation, the low albedo of solid and dark materials, high surface roughness, vehicular traffic, and the use of heat-emitting equipment collectively promote heat retention in urban air and soil. This occurs through greater absorption of short- and long-wave radiation and reduced heat dissipation via evaporation [7].

Two key points merit attention. First, the effects of heat islands are well documented, particularly in large cities. However, smaller cities also experience problems related to increasing urban heat [8,9,10]. Second, most studies on heat islands rely on comparisons between temperature measurements in urban and nearby

rural areas. Such methodological approaches typically consider spatial temperature distributions without incorporating local site characteristics—such as topography, vegetation, and land-use patterns—that directly influence thermal behavior.

In Brazil, this limitation is compounded by the scarcity of meteorological stations across urban areas, necessitating data extrapolation through statistical techniques such as Inverse Distance Weighted (IDW) interpolation and kriging. These methods rely solely on the analyzed variable's values without including additional explanatory parameters [11].

These limitations create a data void and a gap in information on specific urban climates, such as those of the Western Amazon, which are inserted in a region where it is still possible to determine the differences between the environment before and after human occupation, given its degree of preservation.

Through statistical modeling, air-temperature mapping can be achieved by establishing correlations between field-measured temperature data and urban-site characteristics. This approach represents a major advancement in understanding the spatial distribution of air temperature, as it integrates variables that influence the energy balance and shape the urban heat island. This methodology has been successfully applied and validated in several studies [9,10,11,12,13,14,15,16,17].

Modeling has become a recurrent focus in urban climate research, particularly in studies aimed at understanding and diagnosing UHIs. This trend underscores the potential of models to represent the phenomenon and their ability to incorporate landscape heterogeneity, enabling the identification of the unique spatial expressions of the phenomenon in each city where they are applied [11]. The modeling used in this study is empirically based, derived from the statistical relationship between variables in the system under consideration, and provides practical value in describing the phenomena analyzed [5,7,18,19,20,21].

Discussions on the role of modeling in urban climate research, the possibilities offered by existing models, and the pathways for improving diagnostic capacity provide an essential framework for policy planning and the development of intervention tools [7,12,22,23].

In multiple regression analysis, a statistical model is constructed to explain the relationship between independent variables and dependent variables. Once

established, the model enables analysis of the influence of each independent variable and prediction of variations in the dependent variable based on the explanatory variables [24,25]. The combined use of multiple linear regression and geographically weighted statistical approaches at urban and neighborhood scales has produced significant results in understanding how built environments influence UHI formation, as demonstrated by Szymanowski and Kryza [26], László and Szegedi [27], Hofierka et al. [28], and Agathangelidis, Cartalis, and Santamouris [29].

In Amazonian cities, heat intensification resulting from urbanization and urban lifestyles has a considerable impact, given the region's naturally hot and humid climate, which already promotes thermal discomfort. Urban development in this region has often disregarded the potential and limits of local climatic conditions, exposing populations to unfavorable thermal environments.

The creation of cities in the Amazon has followed development policies that imposed spatial and temporal structures designed by state and capital interests, frequently clashing with the social and cultural dynamics of Amazonian populations [30]. Even as the world faces new challenges, the structural logics sustaining capital monopolization, such as the international division of labor and unequal access to development benefits, continue to shape urban realities [31].

In the Amazon region, economic dynamics combine modern and traditional processes within the urban fabric. These cities exhibit the same structural challenges found elsewhere in Brazil, including inequality, poverty, precarious employment, low wages, and informal settlements [31]. In Coari, the onset of oil exploration in the 1980s triggered rapid population growth for which the city was unprepared, lacking adequate infrastructure and territorial planning. The influx of new enterprises and residents, coupled with weak local governance, generated numerous environmental and social problems whose impacts are also reflected in the urban climate, directly affecting the quality of life of residents in Coari.

The research sought a methodology that allowed episodic records from mobile transects, since there is no network of temperature sensors in Coari, while considering the context of the collection points to relate the production of urban space and urban heat island, through modeling. Despite the advances in relation to the application of statistical modeling in urban heat island studies, there are still few applications aimed

at Amazonian cities, especially small ones, which incorporate variables of urban site configuration, land cover and statistics for the analysis of intraurban air temperature.

Study area

The city of Coari lies in the central region of the western Brazilian Amazon rainforest, approximately 363 km from Manaus, the capital of the state of Amazonas (Figure 1). Situated on the right bank of the Solimões–Amazonas River and Lake Coari, the municipality covers an area of 57,970.77 km² and has a population of 70,616, about 70 percent of whom live in the urban area [32].

Due to the beginning of oil activities in the Coari region, the city attracted a migratory flow that increased its population, this process made the city an important center in the urban network of the state. Analyzing the ICU in Coari allowed a theoretical advance for urban climate studies in the region and the analysis of climate processes never examined in comparable contexts.

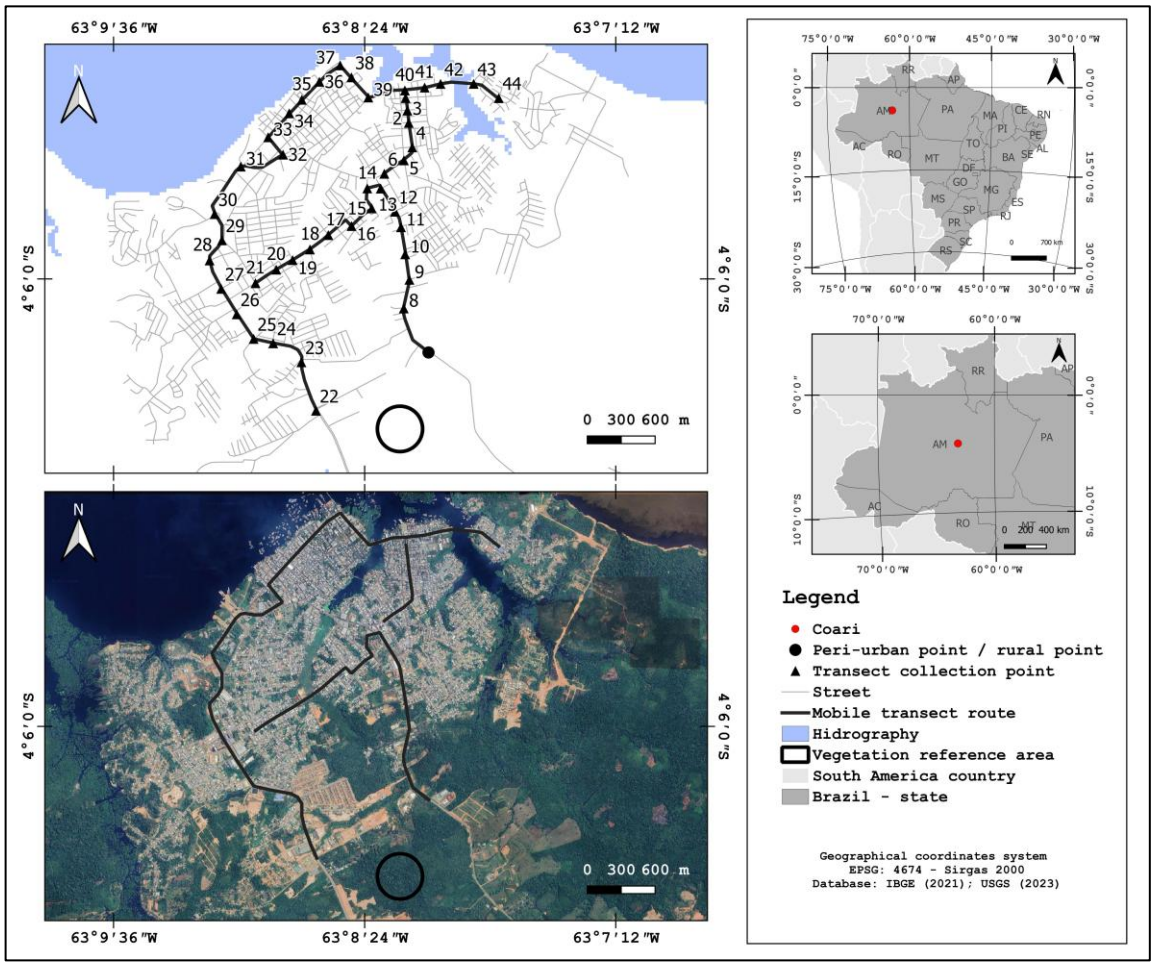


Fig. 1 Location of Coari, Amazonas, Brazil, and distribution of air-temperature recording points along the transectos. Source: IBGE (2021); Google Earth (2023).

The study area has a type Af climate in the Köppen classification—tropical with no dry season [33]. Air temperatures remain high throughout the year, ranging from 22 °C to 33 °C, with little daily and seasonal variation due to high atmospheric humidity and persistent cloud cover (Figure 2).

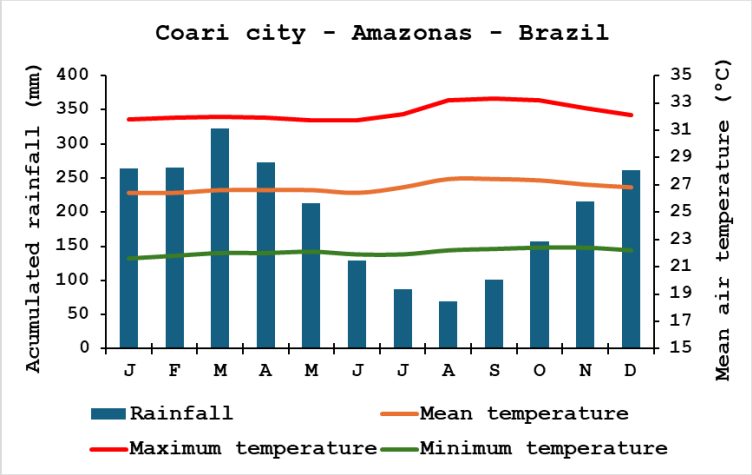


Fig. 2 Coari Climatological Normal (1981-2010). Source: INMET (2010).

It is noteworthy that, as it is an air mass-forming area (MeC – Continental Equatorial Air Mass), the climate variability of the Amazon region is determined by synoptic and large-scale precipitating systems. Thus, for the area, the main systems that generate rainfall are: South Atlantic Convergence Zone (SACZ), Intertropical Convergence Zone (ITCZ), Frontal Systems, Bolivian High (AB), Mesoscale Convective Complexes (MCC) and Instability Lines (LI) [34].

Under conditions of atmospheric stability, the Equatorial Continental Air Mass (MeC), originating and located northwest of the Amazon forest, confers types of weather with high cloudiness, high relative humidity and high air temperature, also favoring the occurrence of rainfall from local convection. Interactions with ocean-atmospheric phenomena, such as El Niño and the Atlantic dipole, are also important factors for climate variability and the occurrence of climate extremes [34].

Methodological procedures

Spatial modeling of air temperature was conducted using multiple linear regression, which enables the creation of maps that represent the relationship between factors influencing local temperature distribution. The procedures were performed in the TerrSet™ software (Clark Labs) using raster data for independent variables (x variables) selected from the literature as relevant to heat island formation. The

modeling followed analytical parameters and statistical reliability criteria to ensure meaningful cartographic representations.

Acquisition of primary data

Variables representing urban-site characteristics, land-cover classes, and spatial organization were selected in accordance with previous studies on urban heat island modeling [9,10,11,12,13,14,16,35,36,37,38].

The selected independent variables included the Normalized Difference Vegetation Index (NDVI), distance from the city center (DCC), elevation, distance from water bodies (DWB) and Local Climate Zones (LCZs), used here as an urban landscape classification instead of an unsupervised cluster-based classification.

NDVI was calculated from Landsat 8 satellite imagery downloaded from the EarthExplorer portal of the United States Geological Survey (USGS). Bands 4 (red) and 5 (near infrared) of the OLI sensors were processed using the arithmetic procedure proposed by Rouse et al. (1974). The index ranges from −1 to 1 (Figure 3) and enables the analysis of spatial temperature variability based on vegetation density and conditions [39].

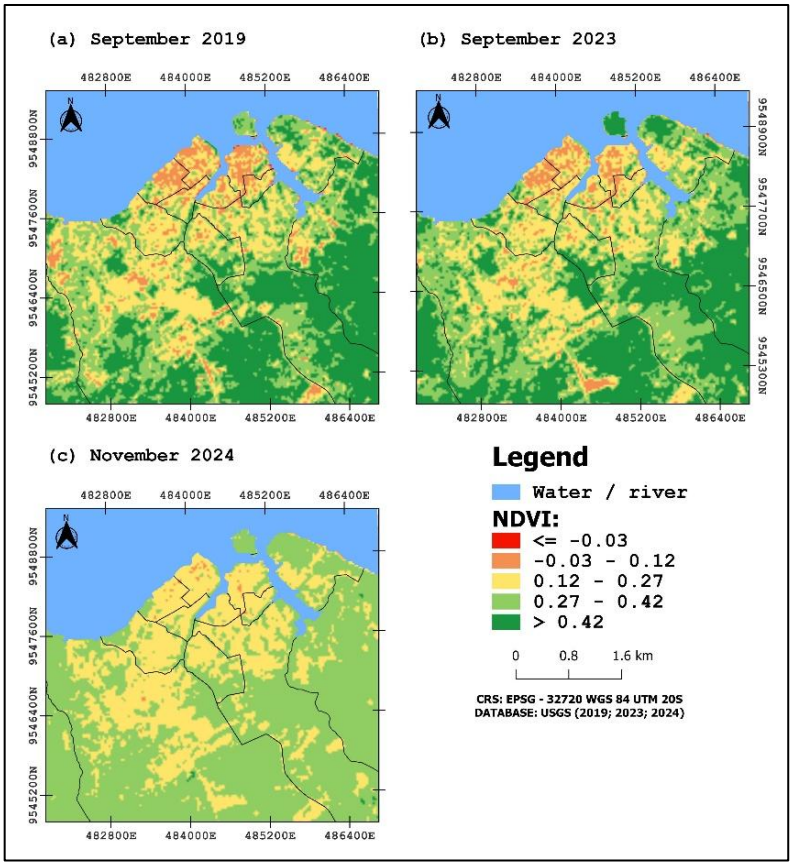


Fig. 3 NDVI imagery used in for spatial modelling. Source: USGS (2019; 2023; 2024)

The NDVI maps represent the dry and rainy seasons, and those with the best quality in terms of minimal cloud cover and temporal proximity to the field data collection dates were selected. Accordingly, NDVI values were calculated for August 12, 2019; August 26, 2023; and November 20, 2024. Elevation data were obtained from the USGS EarthExplorer portal and derived from the Shuttle Radar Topography Mission (SRTM) with a spatial resolution of 30 meters.

Land cover was mapped using the Local Climate Zone (LCZ) classification framework, integrated with Mapbiomas project products through visual interpretation of satellite imagery and field validation. Landscape diversity analysis was performed in QGIS software based on class definitions and land-cover data from Mapbiomas (Collection 8, 2022). The variation in the urbanized area between 2019 and 2024 in Coari was 0.65 km^2, according to land cover data from the Mapbiomas project, which does not compromise the use of the 2022 land cover data for air temperature modeling in other years.

The land cover data from Mapbiomas has a spatial resolution of 30 meters, since it is based on images from Landsat satellites, and was cropped for the urban area of Coari, then it was vectorized using the "polygon raster pixel" tool, which allowed each pixel to be converted into a 30m x 30m polygon. attributes, the pixel value becomes an attribute in the vector, allowing for change, the Mapbiomas coverage class is then reclassified according to the local climate zone class.

The reclassification is performed by applying transparency to the vector layer of the pixels and superimposing it on a recent satellite image, then, based on visual interpretation and field knowledge, the value of the predominant class corresponding to each LCZ is assigned to the polygon of 30m resolution, according to the classification [6], identified in Coari. After all the pixels are reclassified, the 'dissolve' tool is used from the LCZ class column to unify the pixels of the same class into a single feature. Figure 4 summarizes the procedures applied for reclassification.

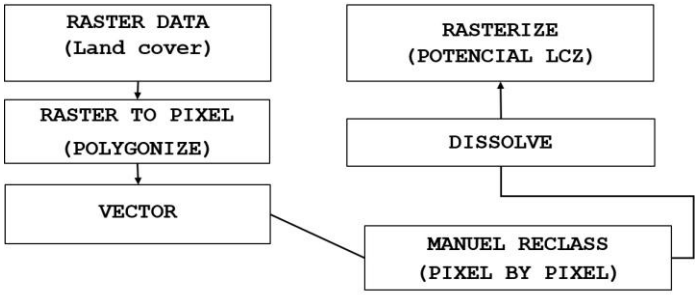


Fig. 4 Stages of land cover classification from potential LCZs. Source: The authors.

Collection 8 of Mapbiomas, used as a reference for the classification of LCZs, has a total of 29 classes for Brazil, for the region of the urbanized area of Coari 9 classes were identified, which were converted to the classes of LCZs. This procedure was the most appropriate in comparison to other classification tools based on the climatic zones [6], such as WUDAPT for example. Due to the size of the city of Coari, other more automated ways of classifying the classes of climatic zones too homogenized, disregarding the heterogeneity of the landscape in the city, this fact demonstrates the limitation of these tools for medium and small cities.

It is worth noting that this methodological intervention is feasible and dialogues with the proposal that intends to be universally applied, inclusive, easy and with screen-level observations. Another aspect refers to the metadata of the climate zones classified for Coari, due to their instrumental limitations, place them as potential local climate zones, requiring measurements of variables such as albedo and sky view factors for a more assertive definition.

In general, the interpretation of the satellite image and the field visits allowed the reclassification of the land cover according to table 1.

Table 1 Land cover classification for potential LCZs. Source: Mapbiomas (2022).

ID	Mapbiomas class	ID	LCZ class
24	Urban area	2	Compact, mid-rise
		3	Compact, low-rise
		3B	Compact, low-rise with Sparse tree vegetation
12, 24	Grassland or Urban area	6	Open Low Elevation
24, 25	Urban area or other non-vegetated areas	9	Large low-rise buildings
12, 24	Grassland or Urban area	8	Sparse buildings
3, 6	Forest formation or Floodable Forest	A	Tree vegetation
12	Grassland	D	Undergrowth

15, 41, 25	Pasture, other temporary crops or other non-vegetated areas	F	Exposed soil or sand
6, 11, 33	River, Lake and Ocean	G	Water

After the land cover reclassification, the vector data is converted to raster format so that it can be incorporated into the set of variables used for statistical modeling, this step is important, since the modeled temperature map is generated by the raster's algebra in the Terset raster calculator.

After organizing the data in matrix format, the analysis is made by moving windows for the classes of local climatic zones, the purpose of its application is to consider the context in which the collection points are inserted for the selection of the land cover classes that most influence the temperature variation, since the air temperature at a given point is affected by the physical properties of the materials and the composition of the land cover in its vicinity. This choice is made based on the correlation coefficient, the classes with the strongest correlation coefficients and the opening window in which it was presented enter the models.

For the LCZ grouped into classes, such as C2 (ZCL 9), C3 (ZCL 6), C4 (ZCL 3B), C5 (ZCL 3), C6 (ZCL 2), C7 (ZCL F), C8 (ZCL 8), C9 (ZCL A) and C10 (ZCL D), the number of pixels of each class in the vicinity of each collection point is calculated, using windows of different sizes. The objective is to verify the relative frequency (in percentage) of each LCZ class in the immediate vicinity of the sampled points [9,14].

For each landscape unit class, moving windows of 3x3 pixels (90 m x 90 m), 5x5 pixels (150 m x 150 m), 7x7 pixels (210 m x 210 m), 9x9 pixels (270 m x 270 m), 13 x 13 pixels (390 m x 390 m) and so on were calculated. The size of the radio of the coverage windows is based on Mapbiomas data, which has a resolution of 30 meters. In practice, this analysis generates several rasters that represent the land cover factors according to the defined buffers, the one that presents the best correlation coefficients enter the algebra of modeling maps.

In Terset 'texture' and 'filter' menus are used to analyze the spatial influence calculated by the moving window, generating a result from the neighborhood, as the data of the coverage classes are qualitative and due to the analysis being carried out

class by class the raster generated is categorical (two classes) and the analysis of the moving window becomes contextual. Figure 5 summarizes the process carried out in the program, the tools calculate and assign to the new raster generated the percentage, density and weighted spatial influence from the central cell of each polygon of the LCZ classes, that is, the discrete variable of the climatic zone is transformed into a continuous morphological variable.

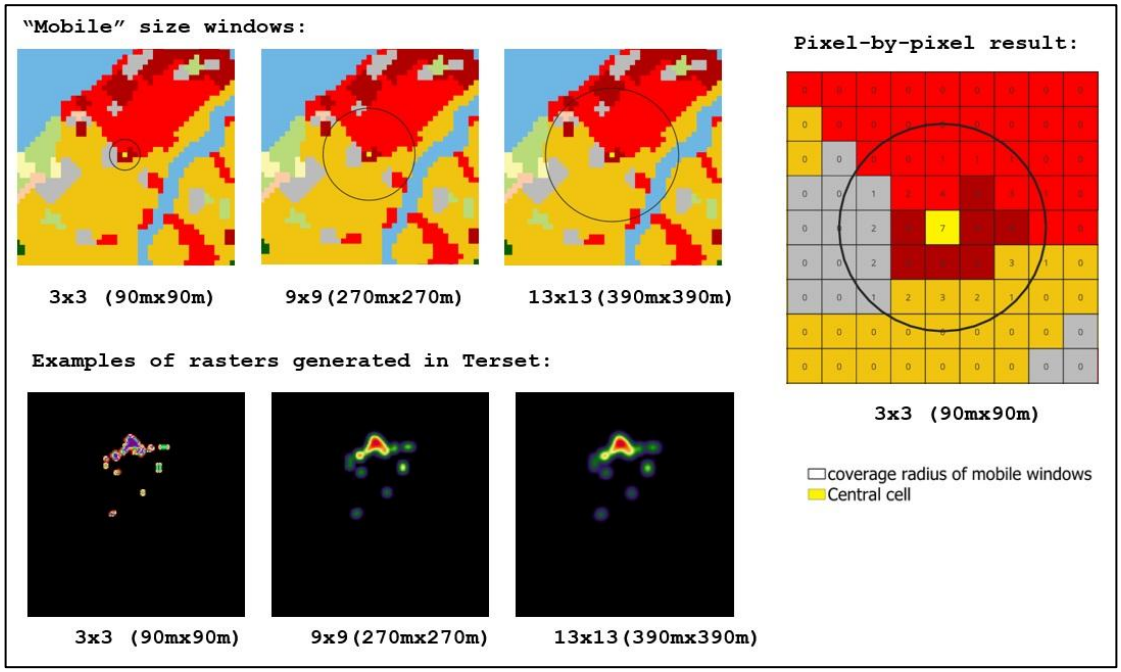


Fig. 5 Scheme of the organization of the raster of the class factors of the local climatic zone.

Then, the correlation of each raster with the measured temperature values is carried out, to find the strongest correlation coefficients and then choose the classes that most influence the measured temperatures. The correlation coefficients of the variables used in the models of each are organized in Table 2. Those that do not have an assigned value were not used in the model due to the weak correlation coefficient.

Table 2 Correlation coefficients of the variables used in the models.

		14/09/19	14/09/19	19/09/23	21/09/23	17/11/24	18/11/24
D. Centre		-0.81	-0.77	-0.68	-0.76	-0.73	-0.7
D. Water		-0.77	-0.7	-0.5	-0.62	-0.58	-0.57
NDVI		-0.74	-0.73	-0.61	-0.53	-0.71	-0.7
LCZ9	mw[3]	61x61	61x61	61x61	61x61	61x61	61x61
	R^2	-0.59	-0.58	-0.74	-0.71	-0.65	-0.64
LCZ3	mw		69x69	61x61			

[3] Mobile Windows

	R^2		0.48	0.42			
LCZ2	mw	61x61	57x57			61x61	61x61
	R^2	0.6	0.43			0.58	0.53
LCZA	mw	21x21	61x61	73x73	61x61	61x61	69x69
	R^2	-0.6	-0.83	-0.8	-0.69	-0.68	-0.66

The variables of distance from the center and distance from water bodies were calculated from the buffer tool in the Terset software, so the variables used in the modeling are represented in figure 6.

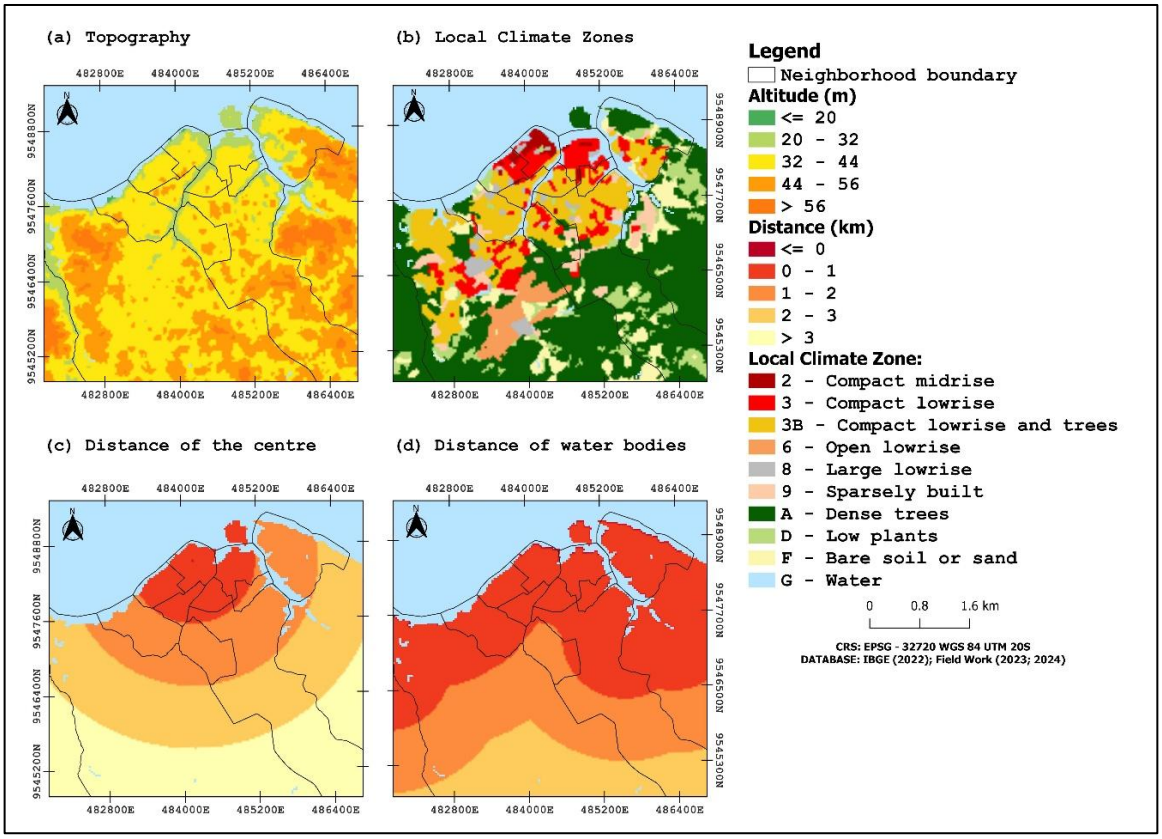


Fig. 6 Independent variables used for statistical modeling. Source: SRTM (2000); [41]; IBGE (2021); [40].

Air temperature data

Due to the lack of a network of weather stations in the city, the air temperature data were collected using mobile transects during field campaigns conducted in September 2019 and 2023 and November 2024 at 8:00 p.m. (GMT −4), standing for the beginning and end of spring.

The choice of months and years for data collection was associated with operational issues and time availability for the execution of fieldwork, but it is noteworthy that the month of September, despite not having the lowest average accumulated rainfall or

the lowest relative humidity, maintains representative atmospheric characteristics of the regional dry season, allowing analysis of the typical climatic conditions of the period.

It is also important to highlight that collections were conducted for 7 days in each field campaign, but only the days that presented the greatest differences in air temperature between the collection points were selected for modelling.

The collections were conducted at 8 pm (local time – UTC -4) because it is the 3rd hour after sunset according to table 1 that organizes the time of sunrise, sunset and duration of the photoperiod on the days of collection in the city of Coari from the solar calculation of NOAA (*National Oceanic and Atmospheric Administration*). The metrics used use the equations from the book 'Astronomical Algorithms' associated with latitude, longitude, and time zone to determine the variables related to solar activity on Earth.

In the table 4 it is possible to see that the length of the days and the time of sunrise and sunset vary little, a fact that occurs because Coari is close to the Equator, about 4° south latitude.

Table 3 Sunrise, sunset and photoperiod in Coari on collection days. Source: NOAA

Date	Sunrise	Sunset	Sunlight duration
14/09/2019	6:05:34	18:10:27	12:10:00
19/09/2019	6:03:14	18:09:13	12:11:08
19/09/2023	5:53:22	18:04:30	12:11:08
21/09/2023	5:52:40	18:04:15	12:11:35
17/11/2024	5:55:18	18:16:28	12:21:10
18/11/2024	5:55:44	18:16:58	12:21:13

The time of 8 p.m. corresponds to an ideal time of day for diagnosing the island of atmospheric heat according to scientific literature, which recommends that measurements occur between 3 and 4 hours after sunset [5,9,42,43].

The intensity or strength of the heat island increases throughout the day as urban surfaces heat up and heat the air, the ICU is more intense at night because urban surfaces release the heat stored during the day more slowly than natural surfaces and during this period decrease cooling [43].

The city stores more heat because infrared radiation remains retained in the complex structure of the urban canopy layer by the multiple reflections between the

ground and the walls of the buildings, favoring less heat loss by nocturnal irradiation [42].

The month of September is one of the months of the period of the year in which the decrease in rainfall totals occurs for the Coari region, while November represents the beginning of the rainy season, which allows a comparison between the intensity of the ICU in the two well-defined seasonal periods, as shown in figure 2. The month of November was selected because it is a transition month, between the rainy and dry periods, which would allow data collection over days without the occurrence of rain, unlike the other months of the rainy season in which rainfall is more frequent.

This methodology is widely used in urban heat island studies to supplement data from fixed weather stations, as an alternative in cities with few or no weather stations, or for microclimate analyses [51, 52].

A Minipa digital thermo-hygrometric sensor (model MT-241A) was used, with a basic accuracy of ±1 °C for temperature (indoor and outdoor) and ± 5% for relative humidity, and a resolution of 0.1 °C and 1 %, respectively. The external sensor and display were mounted on a ½-inch polyvinyl chloride (PVC) rod positioned 1.5 m above the ground.

Data were collected along a route including 44 representative points within the urban network, conducted by motorcycle at a controlled speed of up to 30 km h^{-1}. The routes lasted an average of 45 minutes, with the longest lasting 53 minutes and the shortest 43 minutes, which carried out brief stops of a maximum of 1 minute for each point to stabilize the measured temperature. Correction techniques were not applied to calibrate the regional temperature variation, since the analyses considered the days of atmospheric stability, with little cloud cover and no record of rain or wind.

The calculation of the intensity of the modeled urban heat island for the elaboration of the maps of the figures was carried out from the difference between the values modeled for the urbanized area and the average calculated in a sample cut of 400 meters in diameter of a vegetated area close to the peri-urban reference point, used as point 0 for air temperature in a non-urbanized area.

Multicriteria modeling: selection of independent variables

To define the variables included in each statistical model, a simple linear regression was performed between the air temperature values measured during field campaigns

and the selected geoenvironmental variables to set up correlations. The partial coefficients of determination (R^2) and correlation (r) were used as parameters to figure out the order of entry in the model and to explain the phenomenon mathematically [10].

After selecting the variables based on these parameters, multiple linear regression was applied. With each variable added to the model, variations in the adjusted coefficient of determination (adjusted R^2) were observed.

The degree of relationship between two variables can be expressed through numerical coefficients. Each independent variable is assumed to exert a partial influence on the dependent variable, and therefore each presents a distinct regression coefficient (r). These coefficients are obtained through simple regression between one independent variable and the dependent variable, in a process performed one variable at a time [25,44,45].

The coefficient of determination (R^2) is the proportion of variability in the dependent variable explained by its association with the independent variables. Conversely, the value $1 - R^2$ indicates the unexplained proportion, serving as a relevant analytical indicator. This coefficient ranges from 0 to 1: the closer it is to 1, the greater the explanatory power of the model, showing that the independent variables (X) account for a large share of the dependent variable's variability. In this case, the model is considered adequate; however, when R^2 is close to 0, it reflects low explanatory power [44].

After calculating the r and R^2 values for each independent variable relative to the dependent variable, those showing statistical significance were selected to compose the model. Multiple linear regression was then applied using the stepwise method, which selects the variables with the highest explanatory contribution. Model quality was evaluated using the overall coefficient of determination (adjusted R^2) [44].

Regression analysis begins with a set of observations (x_1, x_2, ..., x_k, y) representing the variables X_1, X_2, ..., X_k, and Y. The dependent variable y (air temperature) is assumed to depend on the corresponding values of X_1, X_2, ..., X_k (elevation, distance from the city center, NDVI), as well as on numerous other factors not included in the model, represented by ε (random error). The formula expressing this relationship is shown below [24,45].

$$y = \alpha + \beta_1 x_1 + \beta_2 x_2 + \beta_3 x_3 + \cdots + \beta_k x_k + \varepsilon \quad (2)$$

Where:

y = dependent variable;

α = intercept (value of the dependent variable when all independent variables are equal to zero);

β 1, β 2, β 3, β k = partial regression coefficients of each variable;

X_1, X_2, X_k = independent variables; and

ε = random error.

Statistical significance of models

The reliability of the model generated was assessed through analysis of variance (ANOVA), the F-test, the adjusted coefficient of determination, and residual analysis. ANOVA determines whether a significant difference exists among the means of the variables being compared. The F-ratio expresses the variation between groups relative to the variation within groups; thus, the higher the F-statistic, the greater the likelihood of rejecting the null hypothesis and accepting the alternative hypothesis [48, 45].

Statistical significance was evaluated at a 5% confidence level (α = 0.05) to confirm or reject the null hypothesis. The null hypothesis (H_0) assumes no linear relationship between X and Y, with variations occurring by chance, whereas the alternative hypothesis (H_1) assumes that the linear relationship between X and Y is significant and not the result of random variation. When the F-statistics of significance is less than α, the statistical significance of the model is confirmed [46].

Another parameter used was the adjusted overall coefficient of determination (adjusted R^2). This coefficient serves as an indicator of model effectiveness because it is robust and resistant—it does not increase with the mere addition of variables, as do multiple R and R^2. The adjusted R^2 compares the explanatory power of regression models, increasing only when a new variable improves the model more than expected and decreasing when a new variable contributes less than expected by chance [10].

Finally, model validity was verified through residual analysis, which examines the differences between the modeled temperature values and those observed at the sampling points in Coari. The residual stands for the difference between the observed and predicted values, reflecting the part of variability not explained by the model structure [24].

The diagram in Figure 7 summarizes the stages and procedures used to organize the products presented in this article.

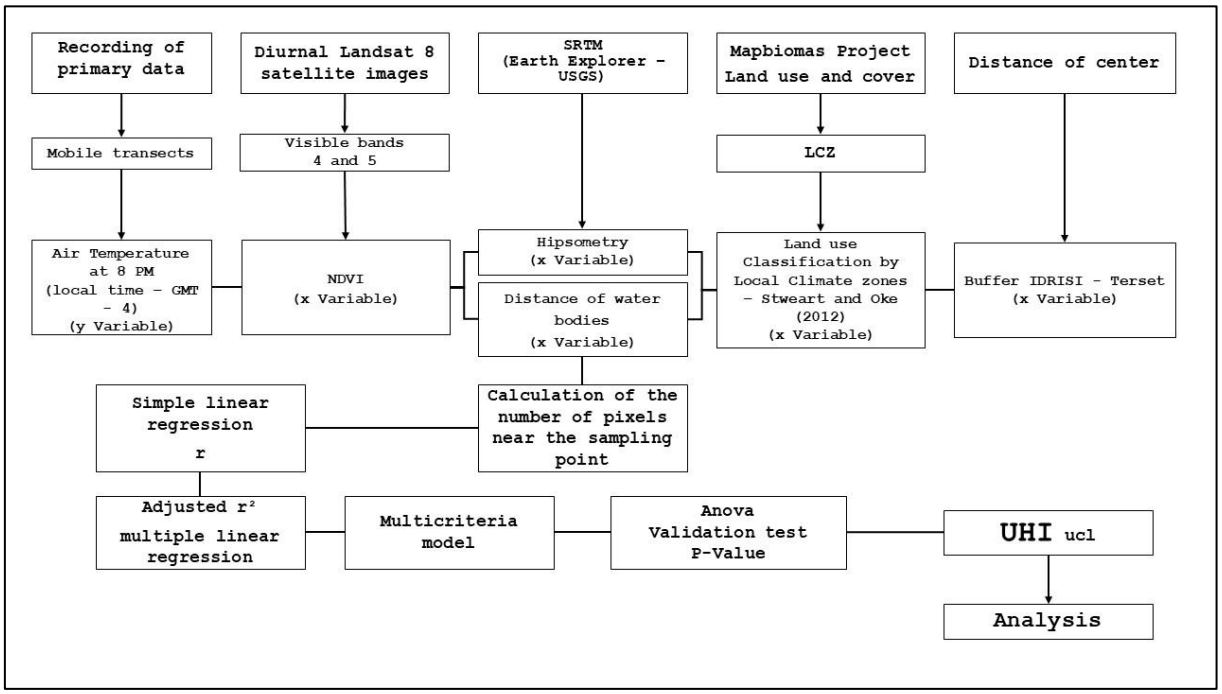


Fig. 7 Data processing phases. Source: elaborated by the authors (2025).

Results

Among the selected variables, distance from the city center and from water bodies, as well as NDVI and Local Climate Zones (LCZs) A, 2, 3, and 9, showed the strongest individual correlations in the paired variable analysis. However, LCZs 2 and 3 were not significant in all models, due to the large areas occupied by these classes, which may reduce statistical variability. Elevation showed a weak correlation with air temperature; its effect on the correlation coefficient was minimal because of the limited altimetric variation within Coari's perimeter. Consequently, elevation was excluded from the air-temperature modeling.

Regarding the landscape unit classes, most sampling points were located within areas classified as LCZ 3B, where temperature variation was relatively small and model sensitivity to this class was the lowest.

Conversely, the model showed stronger correlations for classes with lower spatial representation, precisely because greater variability in modeled temperature was observed within these areas.

Table 4 presents the individual correlation coefficients between recorded air temperature and the variables selected for model construction. Negative values

indicate an inverse relationship between the variables, while the predominance of values above 0.7 provides an important basis for assessing air-temperature patterns in Coari's urban environment using the selected variables.

Table 4 Coefficients of correlation (r2) between air temperature and independent variables

	DCC	DWB	NDVI	LCZA	LCZ2	LCZ3	LCZ9
14/09/2019	- 0.81	- 0.77	- 0.74	- 0.60	0.60		- 0.59
19/09/2019	- 0.77	- 0.70	- 0.73	- 0.83	0.43	0.48	- 0.58
19/09/2023	- 0.68	-0.50	-0.61	- 0.80		0.42	- 0.74
21/09/2023	- 0.76	- 0.62	- 0.53	- 0.69			- 0.71
17/11/2024	- 0.73	- 0.58	- 0.71	- 0.68	0.58		- 0.65
18/11/2024	- 0.70	- 0.57	- 0.70	- 0.66	0.53		- 0.64

Statistical significance and residual analysis

Equation significance was confirmed by the F-test at α = 0.05. Table 5 shows the values used for model validation, specifically the F-values from ANOVA and adjusted determination coefficients for each date. In all models, the F-values calculated from the regressions exceeded the critical F-values for the adopted significance level, indicating that the null hypothesis can be rejected in all cases with 95 percent confidence.

Based on the models' coefficients of determination, it was found that the generated equations explain more than 65% of the variation in temperature, allowing for a meaningful assessment of air temperature in Coari based on the independent variables. The calculation of the mean absolute error (MAE), root mean square error (RMSE), and bias (BIAS) helps quantify the error in the models; these calculations are based on the differences between the measured and modeled values. Table 5 summarizes the values of the statistical variables considered.

1

Table 5 Results for evaluation of the generated model

	F-value	F-test for significance	R^2	Adjusted R^2	MAE	RMSE	BIAS
14/09/2019	35.82	2.36	0.85	0.83	0.4	0.518973	~0.00
19/09/2019	46.11	2.36	0.88	0.86	0.25	0.387585	-0.005
19/09/2023	29.26	2.61	0.75	0.73	0.629545	0.760263	0.51
21/09/2023	19.91	2.45	0.72	0.69	1.152273	1.364388	1.1
17/11/2024	18.81	2.45	0.72	0.68	0.513636	0.724185	~0.00
18/11/2024	20.49	2.61	0.67	0.65	0.540909	0.793865	0.005

Based on the information in the table, the values allowed us to quantify the magnitude of the errors between the modeled and observed values. In the case of 2019, the low ME and BIAS values indicate a smaller magnitude of errors and the absence of a significant systematic trend. In 2023, however, the higher ME and RMSE values, combined with a positive bias, indicated greater dispersion of errors and a tendency for the models to overestimate temperatures. For 2024, the values indicate the absence of a significant trend in the errors and a smaller magnitude of the differences.

The scatter plots illustrate the positive correlation between the estimated and observed values in Coari—that is, the extent to which the model can reproduce the observed values. Based on the results obtained, the data showed coefficients above 0.60 in all analyzed periods between the measured values and those predicted by the models. This indicates that the models were able to consistently track the observed spatial variation in temperature, even though the strength of the relationships varied across the days considered, as shown in Figure 8.

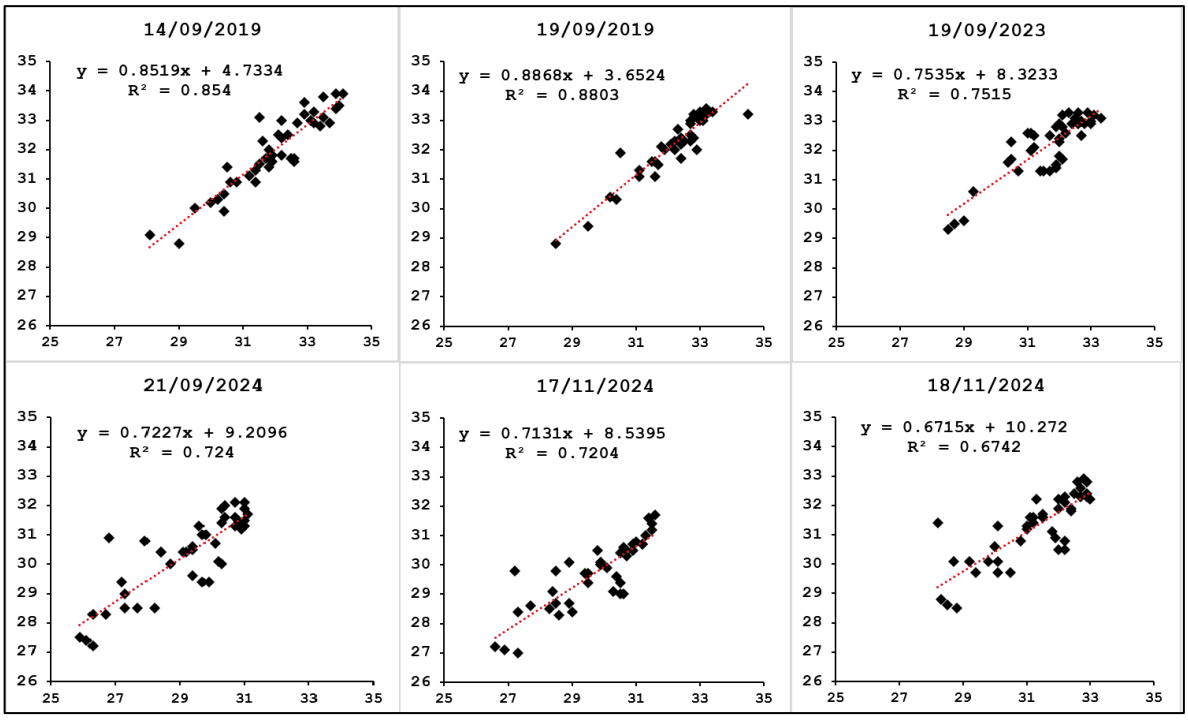


Fig. 8 Relationship between measured and estimated temperatures from the multiple regression models across the different periods analyzed. Source: The authors

Regarding the analysis of observed differences, the residuals of the air-temperature models indicate that the modeled values at the sampling points remained within the approximation margin (between −1 and 1) for most points, as shown in Figure 9.

The residual distribution shows that the models for September 19 and 21, 2023, tended to underestimate the measured values, whereas those for November 17 and 18, 2024, overestimated temperatures between points 27 and 30. It is noteworthy that underestimation predominated from points 41 to 44, possibly reflecting the influence of other variables not included in the present models.

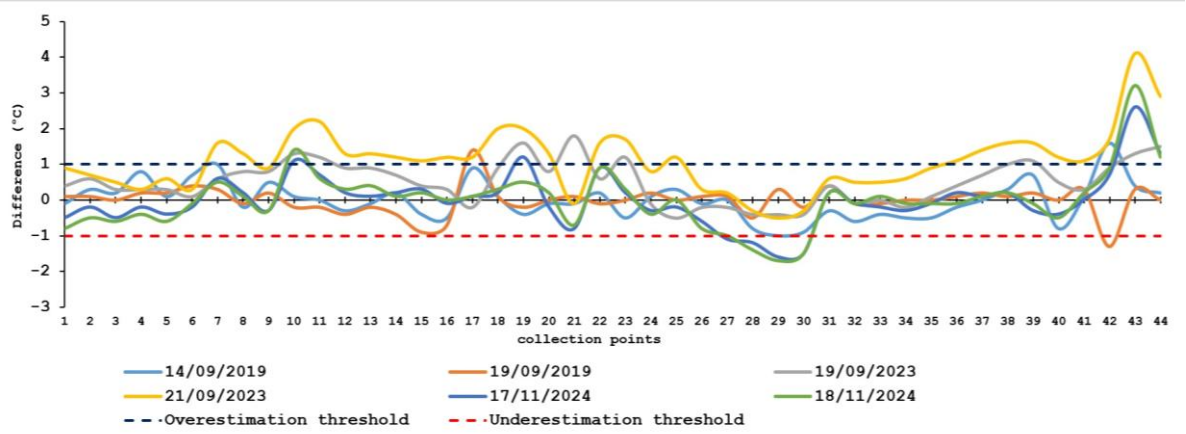


Fig. 9. Differences between measured and modelled air temperature in Coari, Amazonas, Brazil, during 2019–2024. Source: The authors

Spatialization of the heat island

In Coari, September is characterized by a decline in total rainfall. The atmospheric stability resulting from the northward position of the Intertropical Convergence Zone (ITCZ) favors local convection. Consequently, precipitation during this period is mainly convective or associated with the penetration of frontal systems originating from the southern part of the continent. During the sampling days, large-scale atmospheric dynamics on a synoptic scale provided suitable weather conditions for the formation of urban heat islands on the selected days.

The spatial distributions shown in Figure 11 were developed based on the difference between the modeled air temperature at intra-urban points and that measured at a vegetated site near point 7, which was used as a peri-urban reference to analyze the intensity and magnitude of the heat islands. The temperature-difference intervals were classified according to UHI magnitude [42].

Figure 10 presents data collected on September 14 and 19, 2019. During that week, the presence of an anticyclonic flow generated synoptic-scale atmospheric stability and

sustained clear-sky conditions. Under these circumstances, temperature differences of up to 6 °C were recorded between the peri-urban reference point and other areas of Coari, indicating the occurrence of high-magnitude urban heat islands.

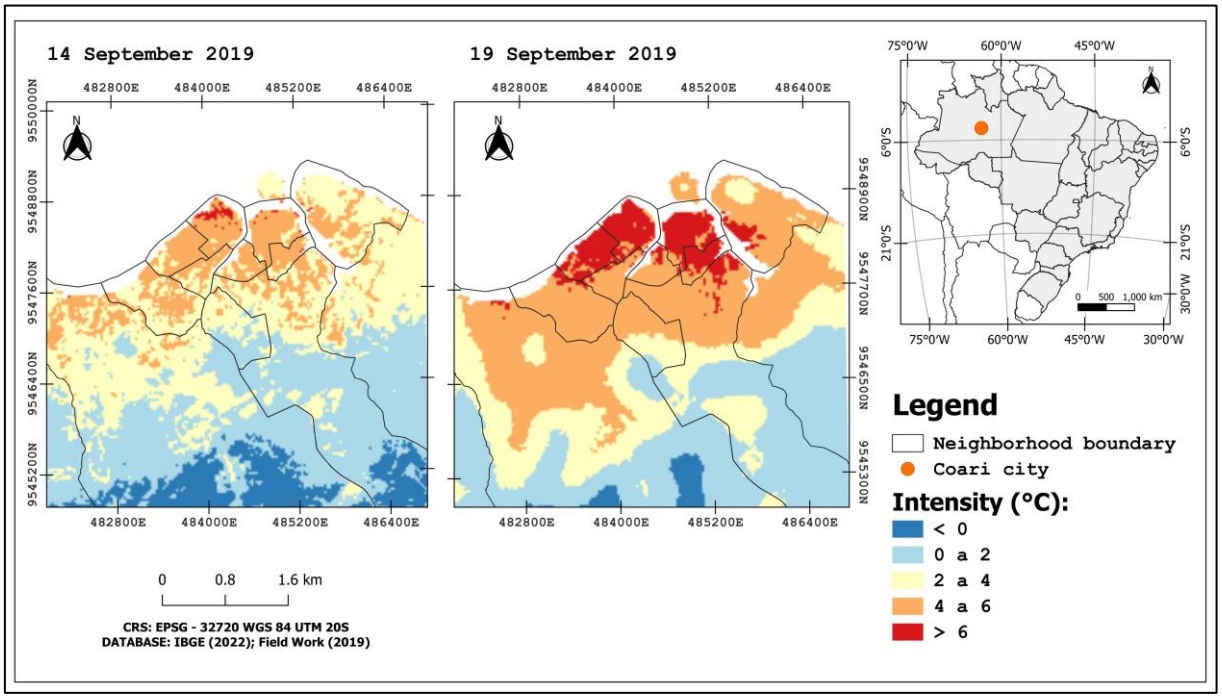


Fig. 10 Spatial distribution of urban heat island intensity for September 14 and 19, 2019, in Coari, Amazonas, Brazil. Source: The authors

During the Coari data collection periods in September 2023 and November 2024, mesoscale convective complexes (MCCs) and local convection were the primary weather systems responsible for intense cloudiness and rainfall on the days they occurred. On other days, the activity of the Continental Equatorial Air Mass (mEc)—the dominant system in the absence of other synoptic-scale influences—produced stable weather conditions with intermittent cloud cover, creating a favorable context for the development of urban heat islands in Coari.

Variations in air temperature across the urban area were directly related to atmospheric dynamics. Rainfall associated with MCCs on September 18 and 20 contributed to the attenuation of the atmospheric heat island effect on those days. On September 19, 2023, however, the heat island was strongly expressed within densely built-up climate zones, with the largest temperature differences concentrated in the city's central area, characterized by minimal vegetation and medium-rise buildings.

On September 21, 2023, a high-magnitude heat island event was recorded, showing the greatest temperature difference among all September 2023 sampling

days. On that date, the city center registered a temperature difference of approximately 5.2 °C. Although nighttime precipitation occurred on September 20, it did not prevent the formation of a strong heat island the following day, likely because the rain occurred late at night, having negligible effect on daytime heating.

In November 2024, which marks the onset of the rainy season in the region, the heat island was concentrated in the city's densely built-up zones. The largest modeled temperature difference occurred on November 18, 2024. NDVI and distance from the city center were significant predictors in the models for this period; however, the coefficient values also suggest the influence of additional variables affecting air temperature in Coari. Figure 11 presents the spatial mappings produced for September 2023 and November 2024.

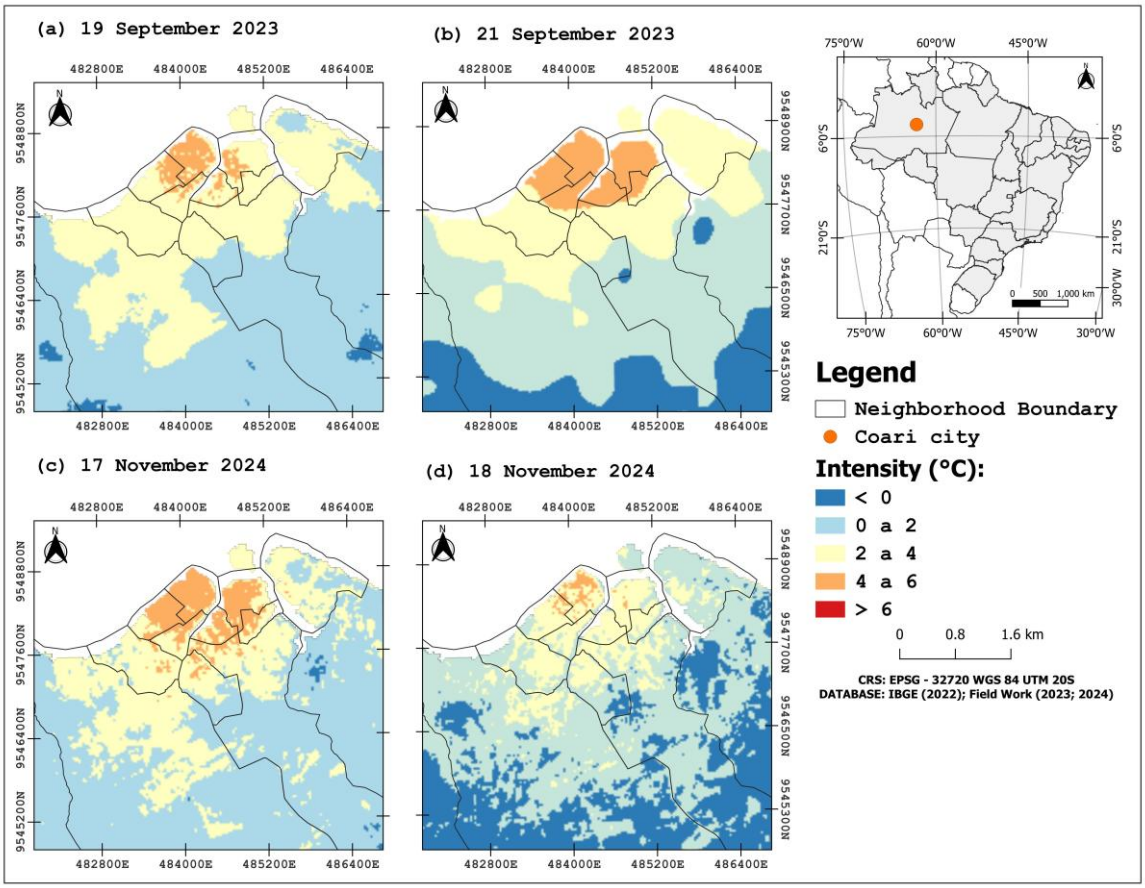


Fig. 11 Spatial distribution of urban heat island intensity for September 2023 and November 2024 in Coari, Amazonas, Brazil. Source: The authors

Air temperature variation as a function of built-up area was clear in the data collected for Coari. A visual comparison between air temperature and the LCZ map shows that zones characterized by high building density—with compact lots and little

or no tree cover, exhibited the greatest temperature differences relative to the peri-urban reference point [38]

Temperature modeling also revealed a heat island distribution pattern in Coari strongly influenced by the city's geometry. Areas classified as LCZ types 2, 3, and 3B concentrated the highest temperature differences observed.

Among the analyzed variables, distance from the city center showed the strongest correlation with temperature. This relationship occurs because the city center corresponds to the most densely built area and, consequently, the warmest sector, resulting in an inverse correlation with distance [9,36].

Vegetation conditions (NDVI) also stood out as one of the variables most strongly correlated with temperature variation [10,13,15,16,35,36].

In Coari, however, this correlation varied among models, due to the low NDVI values in built-up zones and high values in forested areas. Because the temperature sampling points did not extensively include forested areas, the establishment of a stronger correlation was limited by the small number of vegetated sampling sites. The forested areas nearest to the city were those that exhibited the lowest modeled temperature values.

Conclusions

The urban heat island (UHI) in Coari is characterized by a thermal core centered in the downtown area, particularly near the port. Air temperature decreases progressively with distance from the city center, reflecting the moderating influence of surrounding vegetated areas.

The UHI model proved to be an effective tool for analyzing the spatial distribution of temperature across the city. The equations generated explained more than 60% of the observed temperature variability, underscoring the relevance of the selected independent variables in shaping Coari's thermo-hygrometric field.

Statistical modeling confirmed that distance from the city center and land-cover classes exerted a stronger influence on air-temperature distribution than NDVI or elevation.

Future studies should incorporate a broader range of variables related to urban settings and atmospheric dynamics. Parameters such as wind direction and speed,

surface albedo, and land-surface temperature could improve model accuracy. It is important to note, however, that this study faced limitations in acquiring such data due to the lack of specialized equipment and the low quality of available satellite imagery for the region. These constraints are further compounded by persistent cloud cover during the rainy season and smoke from wildfire during the drier months.

Author contributions

LSAF: conceptualization, methodology, formal analysis, investigation, resources, data curation, writing - original draft, writing - review e editing, visualization. LFA: methodology, formal analysis, Writing - review e editing, supervision. MCCTA: conceptualization, writing - review e editing. JCASN: formal analysis, resources, data curation, project administration. NCRA: conceptualization, methodology, formal analysis, resources, writing - original draft, writing - review e editing, supervision, project administration, funding acquisition.

Funding

Part of the data for this study was obtained through the project “Climate Emergency in Amazonian Cities,” funded by the Amazonas State Research Support Foundation (Call for Proposals N° 002/2021 – Case No. 01.02.016301.000067/2021-1). A Master's-level scholarship was awarded to the first author by the same foundation (Graduate Studies Support Program (POSGRAD) - funding code 001).

Data availability Statement

Data will be made available upon request.

Declarations

Ethics statement and consent to participate

Not applicable.

Consent for publication

Not applicable.

Clinical trial number

Not applicable.

Competing interest

The authors declare no competing interests.

References

1. IPCC. 2023. Climate change: Synthesis report. https://www.ipcc.ch/report/sixth-assessment-report-cycle/; 2023.
2. United Nations. World Cities Report 2022. New York: United Nations; 2022.
3. Monteiro CAF. Teoria e clima urbano. In C. A. F. Monteiro F. Mendonça Eds., Clima urbano. Contexto; 2003.
4. Monteiro CAF. Teoria e clima urbano. São Paulo: IGEOG/USP; 1976.
5. Oke T. R., Mills G., Christen A.,, Voogt J. A. Urban climates. 2017. Cambridge University Press.
6. Stewart ID., Oke TR. 2012. Local climate zones for urban temperature studies. Bulletin of the American Meteorological Society. 2012. 93 (12). https://doi.org/10.1175/BAMS-D-11-00019.1
7. Bernard J, Musy M, Calmet I, Bocher E, Keravec P. Urban heat island temporal and spatial variations: Empirical modeling from geographical and meteorological data. Building and Environment. 2017. 125: 423–438. https://doi.org/10.1016/j.buildenv.2017.08.009
8. Weng Q, Yang S. Managing the adverse thermal effects of urban development. Journal of Environmental Management, 2004. 70 (2): 145–156. https://doi.org/10.1016/j.jenvman.2003.11.006
9. Amorim MCCT. Ilhas de calor em cidades tropicais de médio e pequeno porte: teoria e prática. Appris. 2020.
10. Amorim MCCT., Dubreuil V., Teixeira D. C. F., Amorim A. T., Brabant C. Exceptional heat island intensities also occur in medium-sized cities. Urban Climate, 2024, 53. https://doi.org/10.1016/j.uclim.2024.101821
11. Teixeira DCF, Amorim MCCT. Multicriteria spatial modeling. Climate, 2022. 10 (56). https://doi.org/10.3390/cli10040056
12. Foissard X, Dubreuil V, Quénol H. Defining scales of the land use effect to map the urban heat island in a mid-size European city: Rennes France. Urban Climate, 2019. 29: 100490. https://doi.org/10.1016/j.uclim.2019.100490
13. Amorim MCCT., Dubreuil V. Modelagem espacial da ilha de calor urbana em Presidente Prudente SP. Revista Brasileira de Climatologia, 2015. 16. https://doi.org/10.5380/abclima.v16i0.40585
14. Gomes WP, Amorim MCCT., Dubreuil V. Modelagem da ilha de calor urbana aplicada ao ambiente litorâneo – Ubatuba Brasil. Revista do Departamento de Geografia, 2017. 34. https://doi.org/10.11606/rdg.v34i0.133193
15. Dorigon LP, Amorim MCCT. Spatial modeling of an urban Brazilian heat island in a tropical continental climate. Urban Climate, 2019. 28. https://doi.org/10.1016/j.uclim.2019.100461
16. Rampazzo CR., Sant'Anna Neto JL. Episódio do clima urbano em São Carlos/SP. Entre Lugar, 2019. 10 (19): 133–150. https://doi.org/10.30612/el.v10i19.10007
17. Porangaba GFO., Teixeira DCF., Amorim MCCT., Silva MHS., Dubreuil V. Modeling the urban heat island at a winter event in Três Lagoas Brazil. Urban Climate, 2021. 37. https://doi.org/10.1016/j.uclim.2021.100853
18. Yang F, Chen L. Developing a thermal atlas for climate-responsive urban design. Energy and Buildings, 2016. 111: 120–130. https://doi.org/10.1016/j.enbuild.2015.11.047

19. Chen HC, Han Q, Vries B. Modeling the spatial relation between urban morphology, land surface temperature and urban energy demand. Sustainable Cities and Society, 2020. 60: 102246. https://www.sciencedirect.com/science/article/pii/S2210670720304674

20. Han S., Li W., Kwan MK., Miao C, Sun B. Do polycentric structures reduce surface urban heat island intensity? Applied Geography, 2022. 146: 102766. https://doi.org/10.1016/j.apgeog.2022.102766

21. Oukawa GY, Krecl P, Targino AC. Fine-scale modeling of the urban heat island. Science of the Total Environment, 2022. 815, 152836. https://doi.org/10.1016/j.scitotenv.2021.152836

22. Barlow JF. Progress in observing and modelling the urban boundary layer. Urban Climate, 2014. 10, 216–240. https://doi.org/10.1016/j.uclim.2014.03.011

23. Giridharan R, Emmanuel R. The impact of urban compactness, comfort strategies and energy consumption on tropical urban heat island intensity: A review. Sustainable Cities and Society, 2018. 40:677–687. https://doi.org/10.1016/j.scs.2018.01.024

24. Barbetta PA. Estatística aplicada às ciências sociais. UFSC. 2012.

25. Witte RS, Witte JS. Statistics 11th ed.. Pearson. 2017.

26. Szymanowski M, Kryza M. Application of geographically weighted regression. Procedia Environmental Sciences, 2011, 3, 87–92. https://doi.org/10.1016/j.proenv.2011.02.016

27. László E, Szegedi S. A multivariate linear regression model of mean maximum urban heat island. Időjárás, 2015. 119 (3), 409–423. http://real.mtak.hu/id/eprint/74407

28. Hofierka J, Gallay M, Onačillová K, Hofierka Jr J. Physically-based land surface temperature modeling in urban areas using a 3-D city model and multispectral satellite data. Urban Climate, 2020. 31, 100566. https://doi.org/10.1016/j.uclim.2019.100566

29. Agathangelidis I, Cartalis C, Santamouris M. Urban morphological controls on surface thermal dynamics: A comparative assessment of major European cities with a focus on Athens Greece. Climate, 2020. 8 (11): 131. https://doi.org/10.3390/cli8110131

30. Oliveira JA. As cidades da Amazônia: Novas territorialidades e velhas exclusões reencontradas. Caderno Prudentino de Geografia, 199. 21: 53–70. https://revista.fct.unesp.br/index.php/cpg/article/view/7264

31. Castro E. Cidades na floresta. Annablume. 2009.

32. Instituto Brasileiro de Geografia e Estatística. Censo demográfico 2022. Rio de Janeiro: IBGE; 2022.

33. Alvares CA., Stape JL., Sentelhas PC., Gonçalves JL, Sparovek G. Köppen's climate classification map for Brazil. Meteorologische Zeitschrift, 2013. 22 (6), 711–728. https://doi.org/10.1127/0941-2948/2013/0507

34. Fisch G, Marengo JA, Nobre CA. Clima da Amazônia. Climanálise. 1998.

35. Naif SS, Mahmood DA, Al-Jiboori M. H. 2020. Seasonal NDVI responses to air temperature and precipitation in Baghdad. Open Agriculture, 2020. 5 (1):631–637. https://www.degruyterbrill.com/document/doi/10.1515/opag-2020-0065/html

36. Singh P, Verma P, Chaudhuri AS., Singh VK, Rai PK. Evaluating the relationship between urban heat island. International Journal of Environmental Science and Technology, 2024. 21 (3), 3061–3072. https://doi.org/10.1007/s13762-023-05141-y

37. Modi T, Ghosh T, Ali D, Alarifi S, Choudhary N, Kumar P et al. Geospatial evaluation of NDVI and urban heat island. Geomatics Natural Hazards and Risk, 2024. 15 (1). https://doi.org/10.1080/19475705.2024.2356214

38. Sharmin T, Chappell A, Lannon S. 2025. Spatio-temporal analysis of LST NDVI and SUHI. Energy and Built Environment, 2025. 6 (6): 1142–1155. https://doi.org/10.1016/j.enbenv.2024.06.002

39. Amorim MCCT. Spatial variability and intensity frequency of surface heat island in a Brazilian city with continental tropical climate through remote sensing. Remote Sensing Applications: Society and Environment, 2018. 9: 10–16. https://doi.org/10.1016/j.rsase.2017.11.001

40. United States Geological Survey. Landsat 8 imagery, 2023. Reston: USGS; 2023.

41. Mapbiomas. Collection 8: land cover and use maps of Brazil, 2022. São Paulo: Mapbiomas; 2022.

42. García FF. Manual de climatología aplicada: clima, medio ambiente y planificación. Síntesis. 1996.

43. Gartland L. Heat islands: understanding and mitigating heat in urban areas. London: Earthscan; 2010.

44. Landim PMB. Análise estatística de dados geológicos multivariados. Oficina de Textos; 2011.

45. Wilks DS. 2006. Statistical methods in the atmospheric sciences 2nd ed.. Elsevier.

46. Barbetta PA. Estatística aplicada às ciências sociais. Florianópolis: UFSC; 2010.

47. Araújo LF., Amorim MCCT, Dubreuil V. As relações entre as características paisagísticas e a espacialização da ilha de calor urbana de Sinop-MT. In M. C. C. T. Amorim V. Dubreuil Eds., Cidades, clima e vegetação: modelagem e políticas públicas ambientais. 2024. TotalBooks. https://doi.org/10.52632/978.65.88393.62.8

48. Levin J. Estatística aplicada a ciências humanas. Harbra; 1987.

49. Passos RB, Preisser GB, Reboita MS, Mattos EV. Caracterização de um sistema convectivo de mesoescala. Terrae Didática, 15. 2019. https://periodicos.sbu.unicamp.br/ojs/index.php/td/article/view/8653308

50. Rodríguez LR, Ramos JS, Flor FJS., Domínguez SA. Analyzing the urban heat island. Sustainable Cities and Society, 2020. 55, 102027. https://www.sciencedirect.com/science/article/pii/S2210670720300147

51. Vieira M, Vergauwen T, Top S, Hamdi R. Land cover aware temperature correction of bicycle transects. Urban Climate; 2023 50: 101578. https://doi.org/10.1016/j.uclim.2023.101578

52. Zeynali R, Bitelli G, Mandanici E. Mobile data acquisition and processing in support of an urban heat island study. The International Archives of the Photogrammetry Remote Sensing and Spatial Information Sciences. 2023. https://doi.org/10.5194/isprs-archives-XLVIII-1-W1-2023-563-2023